Light emission and finite-frequency shot noise in molecular junctions: From tunneling to contact

Jing-Tao Lü,[1,2,3,*] Rasmus Bjerregaard Christensen,[2] and Mads Brandbyge[2]

[1]*School of Physics, Huazhong University of Science and Technology, 1037 Luoyu Road, Wuhan, China*

[2]*DTU-Nanotech, Department of Micro- and Nanotechnology, Technical University of Denmark, Ørsteds Plads, Bldg. 345E, DK-2800 Kongens Lyngby, Denmark*

[3]*Niels-Bohr Institute, Nano-Science Center, University of Copenhagen, Universitetsparken 5, 2100 Copenhagen Ø, Denmark*

(Received 5 April 2013; revised manuscript received 9 June 2013; published 8 July 2013)

Scanning tunneling microscope induced light emission from an atomic or molecular junction has been probed from the tunneling to contact regime in recent experiments. There, the measured light emission yields suggest a strong correlation with the high-frequency current/charge fluctuations. We show that this is consistent with the established theory in the tunneling regime, by writing the finite-frequency shot noise as a sum of inelastic transitions between different electronic states. Based on this, we develop a practical scheme to perform calculations on realistic structures using nonequilibrium Green's functions. The photon emission yields obtained reproduce the essential feature of the experiments.

DOI: 10.1103/PhysRevB.88.045413 PACS number(s): 72.70.+m, 68.37.Ef, 73.20.Mf, 73.63.Rt

I. INTRODUCTION

When a scanning tunneling microscope (STM) tip is brought towards a metal surface, strong localized plasmon modes develop between the tip and surface, in addition to the propagating surface mode at the metal interface. Under an electric field, the plasmon modes interact with the electrons traversing the gap. This provides an efficient way to excite the plasmon modes electrically, and has become an important topic bridging nanoelectronics and plasmonics.[1–21] Radiative damping of the excited plasmons results in light emission, which can be detected experimentally in the far field at the same or opposite side of the STM tip.[5–13,20] Analyzing the emitted light can provide information about the nanogap. The dependence of light emission on the type of metal, the shape of tip and surface, and on the inserted molecular layer between tip and surface, have all been explored.[14–19,22] Different types of plasmon modes have been detected.[20,21] Most of these experiments are done in the tunneling regime, where the coupling between STM tip and metal surface is weak. Theoretically, it has been established that the excitation of plasmon modes is due to the inelastic electronic transitions taken place near the gap.[23,24]

Recently, STM-induced light emission has been probed during the transition from the tunneling to the contact regime, both for single atom contacts and a C_{60} molecular junction.[25–27] The experimental results suggest a strong correlation between the light emission intensity and the current/charge fluctuations at optical frequencies, and furthermore, show the possibility of controlling light emission by engineering the electronic structure. The established theory in the weak coupling, tunneling regime seems to be inadequate for explaining the experimental results in the strong coupling, contact regime.

A detailed modeling of such experiments needs to take into account the plasmon field distribution near the STM tip, the nonequilibrium electronic structure at high bias, the coupling of the plasmonic field with electrical current, and the propagation of light to the far field.[23,24,28] In this paper, instead of developing a full theory, we focus on the electronic part of the problem. In particular, we study how the change of the electronic structure with tip-position and voltage bias influences the efficiency of plasmonic excitation. To this end, we derive a Fermi-golden-rule like expression for the finite frequency shot noise, and relate it to the theory of STM-induced light emission in the tunneling regime. We then express the result in terms of nonequilibrium Green's functions (NEGF) and develop a practical scheme to perform calculations on realistic structures, using information available from density functional theory based NEGF (DFT-NEGF) transport calculations. We demonstrate how this scheme manage to capture the essential feature of the atomic metal and molecular contact experiments.

II. THEORY

In this section, we briefly summarize the theory of STM-induced light emission in the tunneling regime.[23,24] Then, following Refs. 29 and 30, we introduce an approach to express the finite frequency shot noise in a coherent conductor as a sum of inelastic electronic transitions. We demonstrate how the shot-noise explanation of the light emission in a molecular contact is consistent with the theory in the tunneling regime.

A. Inelastic transition due to electron-plasmon interaction

Following the theory of light emission from STM[23,24] and point contacts,[31] the interaction of the electrical current with the plasmon field in the tip-surface cavity is described by the following Hamiltonian,

$$H_{\rm int} = \frac{1}{c}\int j(r)A(r)d^3r\,, \tag{1}$$

where $j(r)$ is the electron current density operator at position r. The plasmon mode, with frequency, Ω, and spatial distribution, $\xi(r)$, is represented by a vector potential,

$$A(r) = \sqrt{\frac{2\pi\hbar c^2}{V\Omega}}\xi(r)(a+a^\dagger)\,. \tag{2}$$

Here, $a(a^\dagger)$ is the annihilation (creation) operator of the plasmon mode, c is the speed of the light, $\hbar$ is the reduced Planck constant, and V is the normalization volume. In

principle, we may calculate the plasmon mode frequency and field distribution for a given a tip-surface distance. However, this is a daunting task for atomistic first principles theory and we do not consider this problem here. Instead, we focus only on the source of the light emission, and investigate the effect of the nonequilibrium electronic structure on the emission rate. We ignore the spatial distribution of the mode in the xy plane transverse to the current, $\xi(r) = \xi(z)$, and perform the integration over these directions in Eq. (1) and get

$$H_{\rm int} = \frac{1}{c}\int I(z)A(z)dz, \\ = M(a + a^\dagger), \tag{3}$$

where $I(z)$ is the surface current evaluated at z, integrated over the transverse surface. The emitted power from the junction is proportional to the inelastic transition probability due to the interaction between initial(ψ_i) and final(ψ_f) states originating from the tip or surface electrode,

$$P(\Omega) \sim \sum_{i,f}\iint |\langle\psi_f|M|\psi_i\rangle|^2\delta(\varepsilon_i - \varepsilon_f - \hbar\Omega) \\ \times n_F(\varepsilon_i - \mu_i)[1 - n_F(\varepsilon_f - \mu_f)]d\varepsilon_i d\varepsilon_f\,. \tag{4}$$

We employ the normalization, $\langle\psi_i|\psi_j\rangle = \delta_{ij}\delta(\varepsilon_i - \varepsilon_j)$, and filling given by the Fermi-Dirac distributions n_F, corresponding to the initial and final electrodes with Fermi energies given by μ_i and μ_f, respectively. Finally, we will assume that the "diagonal" contributions in the z direction capture the main dependence of the emitted power on the electronic structure of the junction. Thus we get,

$$P(\Omega) \sim \int dz|\xi(z)|^2\sum_{i,f}\iint |\langle\psi_f|I(z)|\psi_i\rangle|^2\delta(\varepsilon_i - \varepsilon_f - \hbar\Omega) \\ \times n_F(\varepsilon_i - \mu_i)[1 - n_F(\varepsilon_f - \mu_f)]d\varepsilon_i d\varepsilon_f. \tag{5}$$

This "diagonal" assumption can clearly not be justified *per se* without concrete knowledge about the spatial distribution of the mode along with the local current operator. However, below we will use a first-principles method in order to calculate without any fitting parameters the light emission using this approximation and compare with the experimental trends.

B. Current, charge fluctuations, and emission rate

Now we show that the Fermi's golden-rule rate in Eq. (5) is closely related to the finite frequency shot noise of the electrical current, which is defined as

$$\langle\langle I_z(0)I_{z'}(t)\rangle\rangle \equiv \langle(I_z(0) - \langle I_z(0)\rangle)(I_{z'}(t) - \langle I_{z'}(t)\rangle)\rangle, \tag{6}$$

where $I(t) = e^{iHt/\hbar}Ie^{-iHt/\hbar}$ is the surface current operator along z in the Heisenberg representation and z/z' are two positions along the transport direction. The positive direction of I_z is defined to be from the surface electrode towards the tip. Since we are dealing with the time dependence explicitly, we put the position variables z, z' as the subindices. The Fourier transform of Eq. (6) gives the noise spectrum,

$$S_{zz'}(\omega) = \int_{-\infty}^{+\infty}\langle\langle I_z(0)I_{z'}(t)\rangle\rangle e^{i\omega t}dt\,. \tag{7}$$

Following Refs. 29 and 30, inserting a complete set of eigenstates into Eq. (7), and doing the Fourier transform, we obtain a golden-rule-type expression for the current noise,

$$S_{zz'}(\omega) = 2\pi\hbar\sum_{\substack{i,f\\ i\neq f}}\iint\langle\psi_i|I_z|\psi_f\rangle\langle\psi_f|I_{z'}|\psi_i\rangle\delta(\varepsilon_i - \varepsilon_f - \hbar\omega) \\ \times n_F(\varepsilon_i - \mu_i)[1 - n_F(\varepsilon_f - \mu_f)]d\varepsilon_i d\varepsilon_f\,. \tag{8}$$

The initial and final states are summed over scattering states from both electrodes. Equation (8) includes both the Nyquist-Johnson (thermal) and shot noise contributions. Since the energy of the emitted light is much larger than the thermal energy ($\hbar\omega \gg k_BT$), only the zero-temperature limit is considered. In this case, besides the zero-point fluctuations, the only contribution is the shot noise,

$$S_{zz'}(\omega) = 2\pi\hbar\sum_{s,t}\int_{\mu_s+\hbar\omega}^{\mu_t}\langle\psi_t|I_z|\psi_s\rangle\langle\psi_s|I_{z'}|\psi_t\rangle d\varepsilon_t\,, \tag{9}$$

with $\varepsilon_s = \varepsilon_t - \hbar\omega$ for positive sample bias $V = V_s - V_t > 0$. We define the upper and lower Fermi levels are at $|eV|/2$ and $-|eV|/2$, respectively. The "diagonal" correlation S_{zz} gives the sum of the transition rates between the initial filled tip scattering states ψ_t, and the final empty surface scattering states ψ_s, with energies ε_t and ε_s, respectively. This illustrates how the finite frequency shot noise can be viewed as inelastic electronic transitions between the tip and surface scattering states. The positive frequency/energy part of the noise spectrum corresponds to the photon emission, relevant to the experiment, and the negative part to the absorption process. We notice that if z and z' are located at the surface and tip electrode, respectively, then according to charge conservation,

$$I_d \equiv \dot{Q}_d = I_z - I_{z'}\,, \tag{10}$$

and therefore, the charge fluctuation in the central molecule/"device" region(d) is given by

$$S_{dd} = S_{zz} + S_{z'z'} - S_{zz'} - S_{z'z}\,. \tag{11}$$

Similarly the fluctuation of the average current $I_a = \frac{1}{2}(I_z + I_{z'})$ is

$$S_{aa} = \tfrac{1}{4}(S_{zz} + S_{z'z'} + S_{zz'} + S_{z'z}). \tag{12}$$

Using the result in this subsection, we can write Eq. (5) as

$$P(\Omega) \sim \int dz\,|\xi(z)|^2 S_{zz}(\Omega), \tag{13}$$

which makes connection between the "old" theory for STM-induced light emission in the tunneling regime and the "new" shot noise argument.

III. NUMERICAL SCHEME

We aim at a formulation targeting the DFT-NEGF approach to atomistic electron transport, such as the SIESTA/TRANSIESTA method[32] and similar methods employing a localized basis set. In these the whole system is separated into a central device region(d), and two electrode regions, here the tip (t) and surface (s) electrodes. The electrodes are represented by the self-energies. In order to directly employ the DFT-NEGF

formalism, we will rewrite Eq. (9) in terms of the device Green's functions and the self-energies (Σ_s, Σ_t) folded into the same device region representing the coupling of the device region to tip and surface electrodes, respectively. By our choice of device region, we effectively define separating surfaces between the regions.

As an example, we now consider the current evaluated at the surface electrode. In order to calculate the surface electrode current fluctuations, $S_{ss}(\omega)$, an explicit expression for the surface current is needed in terms of quantities readily available in the DFT-NEGF calculation. The current matrix I_s, can be written as,[33]

$$I_s = -\frac{ie}{\hbar}[P_s, H] = \frac{ie}{\hbar}(V_{ds} - V_{sd}), \tag{14}$$

where P_s denotes projection into the surface electrode subspace, H is the total Hamiltonian, V_{ds} is the coupling matrix between the device and surface electrode, V_{sd} is its complex conjugate, and e is the electron charge. We ignore electron spin throughout the paper, since it is not relevant. We assume an orthogonal basis set; however, a generalization to the non-orthogonal case is straightforward by a Löwdin transformation.

Next, we evaluate the current matrix element between different scattering states. We start from the Lippmann-Schwinger equation connecting the scattering states and the retarded Green's functions of the whole system $G(\varepsilon)$,

$$|\psi_s(\varepsilon)\rangle = |\phi_s(\varepsilon)\rangle + G(\varepsilon)V_T|\phi_s(\varepsilon)\rangle\,. \tag{15}$$

Here, $|\psi_s(\varepsilon)\rangle$ and $|\phi_s(\varepsilon)\rangle$ are the scattering states from the semi-infinite surface electrode with and without coupling to the device, respectively. Note that ϕ_s is nonzero only in the surface electrode, but ψ_s spans over the whole region including both electrodes and the device. The coupling matrix V_T represent the coupling between the device and the two electrodes, localized near the device-electrode interfaces. Here, $G(\varepsilon)$ is the retarded Green's function of the whole system including the effect of V_T.

Using the projection matrices, $P_t + P_d + P_s = I$, and the fact that $V_T|\phi_s\rangle$ is only nonzero in the device region, it is possible to write the current matrix element $\langle\psi_t(\varepsilon)|I_s|\psi_s(\varepsilon_-)\rangle$ in terms of the device Green's functions and self-energies, where $\varepsilon_- = \varepsilon - \hbar\omega$. Firstly, using $V_{ds} = P_d V_{ds} P_s$, and Eq. (15), we have

$$P_s|\psi_s(\varepsilon_-)\rangle = (I + G_{sd}(\varepsilon_-)V_{ds})|\phi_s(\varepsilon_-)\rangle. \tag{16}$$

Here, $G_{sd} \equiv P_s G P_d$ is a submatrix of the full Green's function G, and G_{dd} is defined correspondingly. Using the relations

$$G_{sd} = g_{ss}V_{sd}G_{dd}, \tag{17}$$

$$\left|\psi_s^d\right\rangle = P_d|\psi_s\rangle = G_{dd}V_{ds}|\phi_s\rangle, \tag{18}$$

$$\Sigma_s = V_{ds}g_{ss}V_{sd}, \tag{19}$$

we get

$$\langle\psi_t(\varepsilon)|V_{ds}|\psi_s(\varepsilon_-)\rangle = \left\langle\psi_t^d(\varepsilon)\right|G_{dd}^{-1}(\varepsilon_-) + \Sigma_s(\varepsilon_-)\left|\psi_s^d(\varepsilon_-)\right\rangle. \tag{20}$$

Note that here g_{ss} is the retarded Green's function of the isolated surface electrode. Similarly, for the second term in Eq. (14), we have

$$\begin{aligned}\langle\psi_t(\varepsilon)|V_{sd}|\psi_s(\varepsilon_-)\rangle &= \langle\psi_t(\varepsilon)|P_s V_{sd} P_d|\psi_s(\varepsilon_-)\rangle \\ &= \langle\psi_t(\varepsilon)|V_{td}G_{dd}^\dagger V_{ds} g_{ss}^\dagger V_{sd} P_d|\psi_s(\varepsilon_-)\rangle \\ &= \langle\psi_t^d(\varepsilon)|\Sigma_s^\dagger(\varepsilon)|\psi_s^d(\varepsilon_-)\rangle.\end{aligned} \tag{21}$$

Defining

$$W_i(\varepsilon_-,\varepsilon) \equiv G_d^{-1}(\varepsilon_-) + \Sigma_i(\varepsilon_-) - \Sigma_i^\dagger(\varepsilon), \tag{22}$$

we finally obtain the desired matrix element

$$\langle\psi_t(\varepsilon)|I_s|\psi_s(\varepsilon_-)\rangle = \frac{ie}{\hbar}\left\langle\psi_t^d(\varepsilon)\right|W_s(\varepsilon_-,\varepsilon)\left|\psi_s^d(\varepsilon_-)\right\rangle. \tag{23}$$

Note that all quantities are projected to the device region and thus depend on the actual splitting into regions.

Using the current matrix element, we can now write the surface current shot noise at zero temperature as

$$S_{ss}(\omega) = \int_\theta \mathrm{Tr}[W_s(\varepsilon_-,\varepsilon)A_s(\varepsilon_-)W_s^\dagger(\varepsilon_-,\varepsilon)A_t(\varepsilon)]d\varepsilon\,, \tag{24}$$

where the integral is defined as

$$\int_\theta \cdot\; d\varepsilon = \theta(|eV| - \hbar\omega)\frac{e^2}{2\pi\hbar}\int_{\hbar\omega-|eV|/2}^{|eV|/2} \cdot\; d\varepsilon, \tag{25}$$

with $\theta(x)$ being the Heaviside step function, $A_s(\varepsilon) = G_d(\varepsilon)\Gamma_s(\varepsilon)G_d^\dagger(\varepsilon) = 2\pi\sum_{i=s}|\psi_i^d(\varepsilon)\rangle\langle\psi_i^d(\varepsilon)|$ is the device spectral function due to scattering states from the surface electrode, similarly for A_t, and $\Gamma_s = i(\Sigma_s - \Sigma_s^\dagger)$. In the same way, we get the tip current noise,

$$S_{tt}(\omega) = \int_\theta \mathrm{Tr}[W_t^\dagger(\varepsilon,\varepsilon_-)A_s(\varepsilon_-)W_t(\varepsilon,\varepsilon_-)A_t(\varepsilon)]d\varepsilon\,, \tag{26}$$

and their cross correlation,

$$\begin{aligned}S_{st}(\omega) &= S_{ts}^*(\omega) \\ &= -\int_\theta \mathrm{Tr}\left[W_s(\varepsilon_-,\varepsilon)A_s(\varepsilon_-)W_t(\varepsilon,\varepsilon_-)A_t(\varepsilon)\right]d\varepsilon\,.\end{aligned} \tag{27}$$

Equations (24)–(27) are our main formal results, where we have written the finite frequency shot noise in terms of the Green's functions and self-energies, readily available from DFT-NEGF calculations. The difference between Eqs. (24) and (26) reveals the position dependence of finite frequency noise. Importantly, they both yield the standard result in the zero-frequency limit.[34]

Assuming constant self-energies (Σ_s, Σ_t), and decoupled eigenchannel transmissions[33] at different energies, $T_n(\varepsilon)$, we arrive at more physically transparent expressions,

$$S_{ss}(\omega) = \sum_n \int_\theta T_n(\varepsilon)[1 - T_n(\varepsilon_-)]\,d\varepsilon\,, \tag{28}$$

$$S_{tt}(\omega) = \sum_n \int_\theta T_n(\varepsilon_-)[1 - T_n(\varepsilon)]\,d\varepsilon\,, \tag{29}$$

valid for positive sample voltages, $V > 0$. The two expressions are exchanged for negative bias. Note that T_n are the channel transmissions calculated for the particular bias, V. We refer to Appendix for the full result of $S_{ss}(\omega)$ at finite temperature. Unfortunately, we are not able to write the cross correlations S_{st} and S_{ts} in terms of the eigentransmissions T_n.

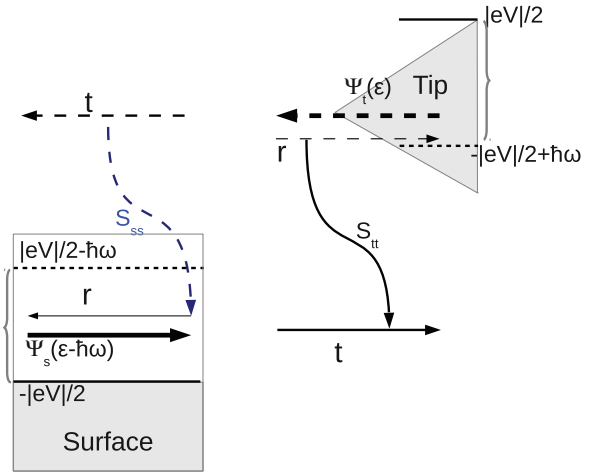

FIG. 1. (Color online) Schematic diagrams showing the two processes contributing to S_{tt} (solid black) and S_{ss} (dashed blue) for positive sample bias, $V > 0$. The curly brackets show two active energy windows for inelastic transitions.

Equations (28) and (29) show that the finite frequency noise is related to the eigenchannel transmission and reflection coefficients at two energy windows. The first energy window corresponds to transmission in the energy range $[\hbar\omega - (eV/2); eV/2]$, the other window is shifted downwards by $\hbar\omega$, $[-eV/2; eV/2 - \hbar\omega]$. We denote these as the active energy windows. The correlation, S_{ss}, corresponds to inelastic transitions taking place at the device-surface interface. For positive sample voltage, $V > 0$, it is proportional to the transmission coefficient of the tip scattering state in the high energy window, and the reflection coefficient of the surface scattering state in the low energy window. The reverse is the case for S_{tt}. Schematic diagrams of these two processes are shown in Fig. 1.

IV. RESULTS

Now we apply the method outlined above to calculate the light emission from the STM resembling two recent experiments where the tip is brought into contact with (i)a Ag adatom on a Ag(111) surface,[26] and (ii) a C_{60} molecule a Cu(111) surface.[27] In the experiments, two type of photons with energy smaller and larger than the applied bias are detected. They are attributed to one- and two-electron process, respectively. Here, we focus only on the former. We used the SIESTA/TRANSIESTA code[32,35] with the generalized gradient approximation (GGA-PBE) for exchange and correlation.[36] For the Ag system, we use a single-ζ polarized basis-set for the Ag atoms. For the C_{60} system, we use a double-ζ basis-set for the carbon atoms, and a single-ζ basis set for the bulk electrode Cu atoms. For both systems, to accurately describe the surface and/or the chemical bonding with the C_{60}, an optimized diffuse basis set was applied for surface layer atoms and the tip.[37]

A. Ag adatom on Ag(111)

In Ref. 26, STM-induced light emission from a Ag-Ag(111) junction has been probed from tunneling to contact regime. The photon yield (roughly emission probability per electron) develops a plateau in the tunneling regime, and has a kink near the conductance quantum upon contact. These results

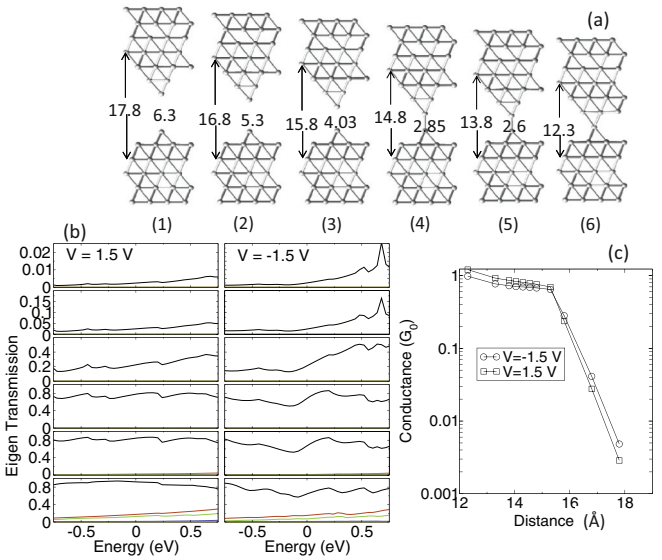

FIG. 2. (Color online) (a) A subset of structures used in the calculation, going from tunneling to contact. In the final structure, one tip atom is pushed aside when forming contact. The two surface layers, the tip and the adatom are relaxed at zero bias for each structure. The numbers show the distance between the two fixed layers and between the tip-adatom in units of Å. (b) Transmission eigenchannels at $V = V_s - V_t = \pm 1.5$ V, going from tunneling to contact (top to bottom), for the structures shown in (a). (c) The average conductance as a function of surface layer separation, showing the transition from tunneling to contact.

suggest possible correlation between photon emission and current shot noise.

To simulate this experiment, we have studied a similar setup: Ag adatom on Ag(111) surface. Figure 2(a) shows a subset of the structures used in the calculations, going from tunneling to contact regime. A 4×4 surface unit cell were used, together with $2 \times 2/5 \times 5$ surface k points to sample electronic structure/transmission. We relaxed the two surface layers, the tip and the adatom at zero bias. After the relaxation, transport calculations were done for a bias of $V = \pm 1.5$ V. Figure 2(b) shows the transmission eigenchannels for the structures in Fig. 2(a). From Fig. 2(b), it is evident that, (i) there is only one dominate transmission eigenchannel, and (ii) there is a small asymmetry in the transmission for the two bias polarities. Figure 2(c) shows the change of the average conductance when going from tunneling to contact on a logarithmic scale. In the tunneling regime, the conductance depends exponentially on the tip-atom distance, while it develops to a plateau upon contact as typically seen in experiments.[26]

The emission rate (proportional to the shot noise power) was evaluated for a plasmon energy of $\hbar\Omega = 1.2$ eV using Eq. (9), or equivalently Eqs. (24)–(26). In order to map out the spatial distribution, the emission rate were calculated for the surface current defined at 6 different interfaces, shown in Figs. 3(a) and 3(b). From these calculations, we observe that the emission rate does not change significantly for interfaces in the same electrode, while they are quite different for the two electrodes, and for the tip-adatom interface.

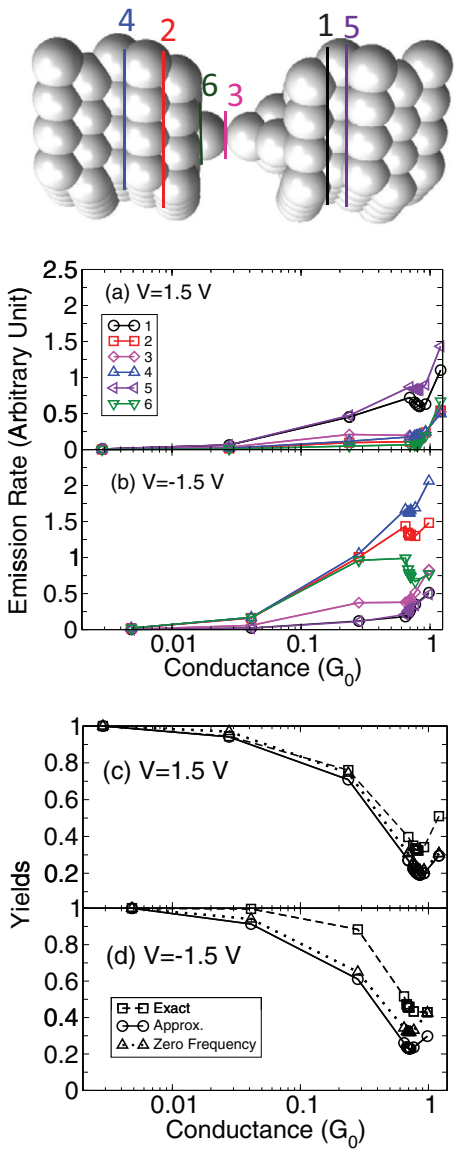

FIG. 3. (Color online) (a) and (b) Calculated noise power (or emission rate) S_{zz} from Eq. (9) for I_z defined through six different surfaces, shown above, for plasmon energy $\hbar\Omega = 1.2$ eV. (c) and (d): Calculated yields $Y = P/\langle I\rangle$, normalized with respect to the first point. The power P is the averaged noise power over the 6 different surfaces (squares). Also shown are the results from average of S_{ss} and S_{tt} using the approximated expressions Eqs. (28) and (29) (circles), and from the zero-frequency noise calculation used in Ref. 26 (triangles). All of them give qualitatively similar results.

To relate the emission rates to the intensity of light emission, we need to do an average of the surface currents, taking into account the spatial distribution of the plasmon mode, $\xi(z)$. Since we do not have specific knowledge about the mode we will choose to do it in the simplest possible way here. Firstly, we take the equally weighted average of all the surface layers [e.g., $\xi(z) =$ constant]. Secondly, as mentioned above, we will use Eq. (5) instead of Eq. (4), so we ignore the cross terms involving surface current at different positions.

We have two comments regarding the approximations. (i) In reality, the plasmon field distribution may change with the tip-surface distance. In the tunneling regime, we expect a high weighting-factor in the region between the tip-surface gap. On the other hand, upon contact, due to the high conductance, we expect the field distribution to spread out into both electrodes.[38,39] Study of this distance-dependent field distribution is an interesting problem by itself, and is beyond the scope of present paper. (ii) We actually tried to include some of the cross terms using Eq. (27), and only see slight change of the final results. But it is computationally too expensive to include all of them.

The final results for the photon yields $Y = P/\langle I\rangle$, normalized over the first point, for the two bias polarities are shown in Figs. 3(c) and 3(d). Here the power P is proportional to the emission rate averaged over six different surfaces. $\langle I\rangle$ is the average current. In Figs. 3(c) and 3(d), we also show results from the approximate calculation using Eqs. (28) and (29), and from the zero-frequency noise employed in Ref. 26. We see that the qualitatively trends are similar for all these calculations: a plateau in the tunneling regime, and the development of a dip at contact around the fully transmitting single channel for $G = 1G_0$, consistent with the experiments.[26]

The agreement between different approximations can be understood from the eigentransmission plotted in Fig. 2(b): (i) in the tunneling regime, there is only one eigenchannel. The eigentransmission is rather small and scales logarithmically with the distance in the whole energy range. Consequently, the distance dependence of the photon yields is encoded in the reflection coefficient $R = 1 - T \approx 1$. As a result, the photon yields show a rather weak dependence on the distance. (ii) In the contact regime, the eigentransmission is rather flat in the whole bias window. From Eqs. (28) and (29), we expect that the finite frequency shot noise shows weak position dependence, and becomes similar to the zero-frequency one.

B. C_{60} on Cu(111)

In Ref. 27, STM-induced light emission from a C_{60} molecule sitting on the reconstructed Cu(111) surface was studied in the tunneling and contact regime. It was found that the C_{60} molecule modifies the photon yields drastically. Especially, a strong bias polarity dependence is observed, indicating the effect of localized molecular resonance on the light emission property.

To simulate this experiment, we used a 4×4 surface unit cell and $2 \times 2/10 \times 10$ surface k points in order to sample the electronic structure/transmission. Due to the surface reconstruction in the experiments[27,40] the two first surface layers and tip were relaxed at zero bias to 0.02 eV/Å at different tip positions. Thus, we do not capture the abrupt jump-to-contact observed in the experiment at finite negative bias in our calculations. Figure 4 shows the five different structures considered in the calculations, together with the transmission eigenchannels at $V = \pm 1.5$ V. Different from the Ag system, when making the contact, there are now mainly three contributing eigenchannels.

As in the experiment, we observe different emission rates for the two bias polarities [see Figs. 5(a) and 5(b)]. For positive sample bias, the magnitude at four different surfaces is comparable. But for the negative bias, the fluctuations near the surface electrode are four times larger than that of the tip

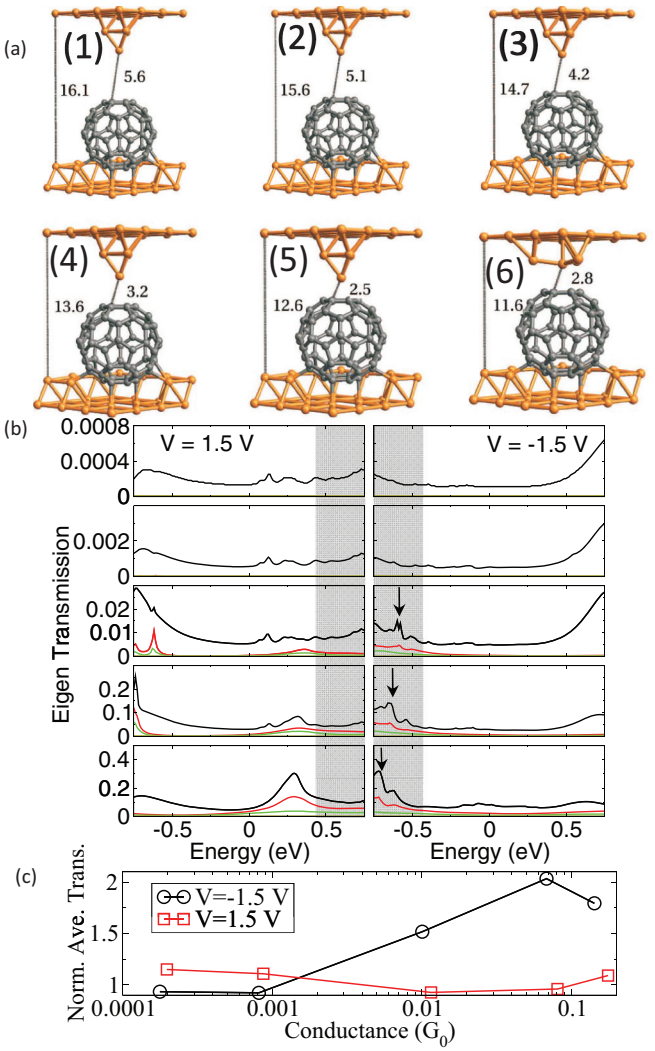

FIG. 4. (Color online) (a) All structures considered in the calculation. In structure 6 a deformation of the tip occurred and has been disregarded in the following. The two surface layers, C_{60} and the tip were relaxed at zero bias for each electrode separation. (b) Transmission eigenchannels at $V = \pm 1.5$ V for the structures shown above. The shaded areas are the active energy windows contributing to S_{ss}. (c) The average transmission in the active energy window [shaded areas in (b)], normalized over that in the whole bias window [−0.75–0.75] eV. The increase from tunneling to contact at $V = -1.5$ V is due to the appearance of HOMO level (peak in the shaded region).

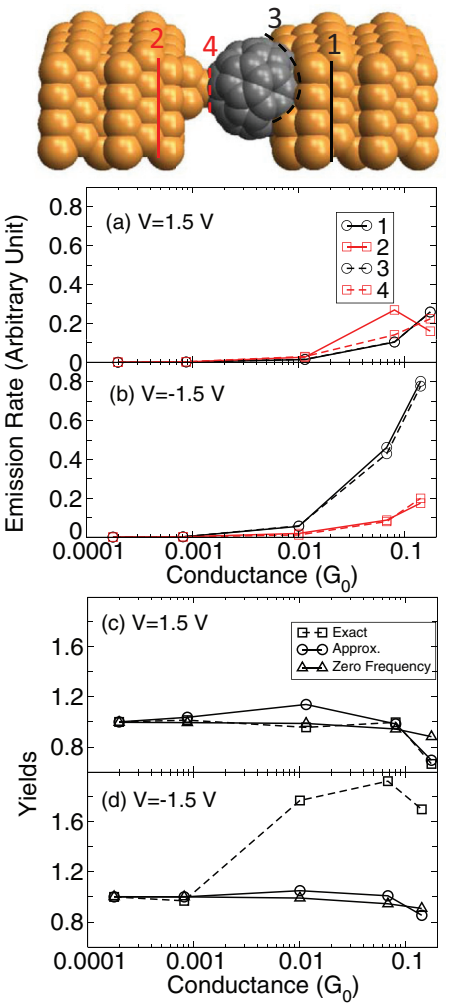

FIG. 5. (Color online) (a) and (b) Similar to Figs. 3(a) and 3(b), calculated emission rates at four different surfaces for the C_{60} system using $\hbar\Omega = 1.2$ eV at $V = \pm 1.5$ V. (c) and (d) Similar to Figs. 3(c) and 3(d).

electrode. Consequently, the calculated yields show different trends at negative and positive bias when going from tunneling to contact, as shown in Figs. 5(c) and 5(d). These results can be explained as a consequence of the appearance of the HOMO level in the bias window, as discussed in Ref. 27. When the HOMO level enters the bias window, the occupied charge begins to fluctuate. This generates new available final states for inelastic transitions, which contribute to high-frequency noise at the plasmon frequency. Since the molecule couples better to the surface than the tip, the charge fluctuations are compensated mainly by the surface-current fluctuations. This allows us to understand the results qualitatively by looking at the surface current fluctuations. In the single channel, small transmission case, we can ignore the $1 - T$ term in Eqs. (28) and (29). So the photon yield due to surface current fluctuation can be characterised by the ratio of the average transmission in the active window (shaded region in Fig. 4) to that in the whole bias window. We plotted this normalized average transmission in Fig. 4(c) and observed a sudden increase upon contact.

Comparing the two systems, we can see that the main difference between them is whether spatially localized molecular resonance participates in the light emission process or not. (1) For the Ag system there are no such localized resonances and the transmission spectrum is weakly energy dependent. The behavior of the finite frequency noise is similar to that at zero-frequency. So the experimental results can basically be understood by looking at the zero-frequency noise, as has been done in Ref. 26. (2) On the other hand for the C_{60} system, at negative bias, the C_{60}-HOMO level enters into the active window upon contact, modifies the transmission in there, and enhances the shot noise power. From this study, we can see that molecular level engineering provides an efficient way to control the light emission property of STM junctions. Along these lines we note that very recent STM

experiments using the photon-map technique indicate that individual molecular resonances can play a determining role ("gate") for the emission process.[22]

V. CONCLUSIONS

We have developed a practical scheme to calculate the finite-frequency shot noise of the electrical current through a coherent molecular conductor within a DFT-NEGF approach. By a spatial average, we re-produce qualitatively the essential features of two recent experiments, confirming the hypothesis that the current/charge fluctuations are the energy source of STM-induced light emission from molecular junctions, going from tunneling to contact. Furthermore, by writing the shot noise expression into a Fermi-golden-rule form, we have established a connection with the theory of light emission in the tunneling regime, based on inelastic electronic transitions. The relation between shot noise power and light emission intensity makes it possible to understand qualitatively the light emission property of atomic/molecular junctions with the help of its eigentransmission spectrum.

Here, we have focused on the source of the light emission, which is the inelastic electronic transitions induced by current. However, to get a quantitative understanding of the experimental results, in a semiclassical model of the electron-plasmon coupling, the following questions have to be addressed: (1) the spatial field distribution of different plasmon modes near the STM tip and (2) their detailed coupling with the current. These questions are also important if we want to distinguish the localized gap mode from the propagating surface mode. Recent experiments showed that the tunneling electrons can couple to both types. An alternative way to proceed is to perform time dependent DFT calculations. So far, model structures have been considered[41] with this approach. However, it is very challenging to perform calculations on realistic structures involving coupling to the metallic surfaces in order to approach the experiments.

ACKNOWLEDGMENTS

We thank R. Berndt and N. Schneider for insightful discussions and the Danish Center for Scientific Computing (DCSC) for providing computer resources. J. T. Lü is supported by the Fundamental Research Funds for the Central Universities, HUST:2013TS032.

APPENDIX: FREQUENCY DEPENDENT NOISE AT FINITE TEMPERATURE

At finite temperature, to evaluate the surface current correlation, we need all the matrix elements. The other three read

$$\langle\psi_s(\varepsilon)|I_s|\psi_t(\varepsilon_-)\rangle = -\frac{ie}{\hbar}\langle\psi_s(\varepsilon)|W_s^\dagger(\varepsilon,\varepsilon_-)|\psi_t(\varepsilon_-)\rangle,$$

$$\langle\psi_t(\varepsilon)|I_s|\psi_t(\varepsilon_-)\rangle = \frac{ie}{\hbar}\langle\psi_t(\varepsilon)|\Sigma_s(\varepsilon_-) - \Sigma_s^\dagger(\varepsilon)|\psi_t(\varepsilon_-)\rangle,$$

$$\langle\psi_s(\varepsilon)|I_s|\psi_s(\varepsilon_-)\rangle = \frac{ie}{\hbar}\langle\psi_s(\varepsilon)|\Sigma_t^\dagger(\varepsilon) - \Sigma_t(\varepsilon_-) - \omega I|\psi_s(\varepsilon_-)\rangle.$$

Assuming a constant self-energy, for positive sample bias, we have the full result for surface current noise at finite temperature

$$S_{ss}(\omega) = \frac{e^2}{2\pi\hbar}\sum_{\alpha\beta} C_{\alpha\beta}(\omega)\Delta n_F^{\alpha\beta},$$

with

$$C_{tt}(\omega) = \int \mathrm{Tr}\left[T(\varepsilon)T(\varepsilon_-)\right]\Delta n_F^{tt}d\varepsilon,$$

$$C_{ss}(\omega) = \int \mathrm{Tr}\left[(\omega I - i\Gamma_t)A_s(\varepsilon_-)(\omega I + i\Gamma_t)A_s(\varepsilon)\right]\Delta n_F^{ss}d\varepsilon,$$

$$C_{st} = \int \mathrm{Tr}\left[(I - T(\varepsilon))T(\varepsilon_-)\right]\Delta n_F^{ts}d\varepsilon,$$

$$C_{ts} = \int \mathrm{Tr}\left[(I - T(\varepsilon_-))T(\varepsilon)\right]\Delta n_F^{ts}d\varepsilon,$$

where

$$\Delta n_F^{\alpha\beta} = n_F(\varepsilon,\mu_\alpha)[1 - n_F(\varepsilon_-,\mu_\beta)].$$

The above result includes both the Nyquist-Johnson (thermal) and the shot noise. Notice the different form of C_{ss} from C_{tt}. It is related to the complex reflection coefficients in the scattering approach discussed by Büttiker.[42] Physically, it means that even when the transmission is zero, there still could be fluctuations at the surface electrode at finite temperature.

*jtlu@hust.edu.cn

[1] A. Nitzan and M. Galperin, Phys. Chem. Chem. Phys. **14**, 9421 (2012).
[2] C. Chen, C. A. Bobisch, and W. Ho, Science **325**, 981 (2009).
[3] D. R. Ward, F. Huser, F. Pauly, J. C. Cuevas, and D. Natelson, Nat. Nanotechnology **5**, 732 (2010).
[4] J. Kern, S. Gromann, N. V. Tarakina, T. Hckel, M. Emmerling, M. Kamp, J.-S. Huang, P. Biagioni, J. C. Prangsma, and B. Hecht, Nano Lett. **12**, 5504 (2012).
[5] J. K. Gimzewski, J. K. Sass, R. R. Schlitter, and J. Schott, Europhys. Lett. **8**, 435 (1989).
[6] X. H. Qiu, G. V. Nazin, and W. Ho, Science **299**, 542 (2003).
[7] Z.-C. Dong, X.-L. Guo, A. S. Trifonov, P. S. Dorozhkin, K. Miki, K. Kimura, S. Yokoyama, and S. Mashiko, Phys. Rev. Lett. **92**, 086801 (2004).
[8] E. Cavar, M. C. Blum, M. Pivetta, F. Patthey, M. Chergui, and W.-D. Schneider, Phys. Rev. Lett. **95**, 196102 (2005).
[9] T. Uemura, M. Furumoto, T. Nakano, M. Akai-Kasaya, A. Salto, M. Aono, and Y. Kuwahara, Chem. Phys. Lett. **448**, 232 (2007).
[10] C. W. Marquardt, S. Grunder, A. Blaszczyk, S. Dehm, F. Hennrich, H. von Lohneysen, M. Mayor, and R. Krupke, Nat. Nanotechnology **5**, 863 (2010).

[11]G. Hoffmann, L. Libioulle, and R. Berndt, Phys. Rev. B **65**, 212107 (2002).
[12]X. Tao, Z.-C. Dong, J. L. Yang, Y. Luo, J. G. Hou, and J. Aizpurua, J. Chem. Phys. **130**, 084706 (2009).
[13]N. L. Schneider, F. Matino, G. Schull, S. Gabutti, M. Mayor, and R. Berndt, Phys. Rev. B **84**, 153403 (2011).
[14]R. Berndt, J. K. Gimzewski, and P. Johansson, Phys. Rev. Lett. **67**, 3796 (1991).
[15]R. Berndt and J. K. Gimzewski, Phys. Rev. B **48**, 4746 (1993).
[16]R. Berndt, R. Gaisch, J. K. Gimzewski, B. Reihl, R. R. Schlittler, W.-D. Schneider, and M. Tschudy, Science **262**, 1425 (1993).
[17]J. Aizpurua, S. P. Apell, and R. Berndt, Phys. Rev. B **62**, 2065 (2000).
[18]Y. Zhang, X. Tao, H. Y. Gao, Z.-C. Dong, J. G. Hou, and T. Okamoto, Phys. Rev. B **79**, 075406 (2009).
[19]F. Geng, Y. Zhang, Y. Yu, Y. Kuang, Y. Liao, Z. Dong, and J. Hou, Opt. Express **20**, 26725 (2012).
[20]T. Wang, E. Boer-Duchemin, Y. Zhang, G. Comtet, and G. Dujardin, Nanotechnology **22**, 175201 (2011).
[21]P. Bharadwaj, A. Bouhelier, and L. Novotny, Phys. Rev. Lett. **106**, 226802 (2011).
[22]T. Lutz, C. Große, C. Dette, A. Kabakchiev, F. Schramm, M. Ruben, R. Gutzler, K. Kuhnke, U. Schlickum, and K. Kern, Nano Lett. **13**, 2846 (2013).
[23]P. Johansson, R. Monreal, and P. Apell, Phys. Rev. B **42**, 9210 (1990).
[24]B. N. J. Persson and A. Baratoff, Phys. Rev. Lett. **68**, 3224 (1992).
[25]G. Schull, N. Neel, P. Johansson, and R. Berndt, Phys. Rev. Lett. **102**, 057401 (2009).
[26]N. L. Schneider, G. Schull, and R. Berndt, Phys. Rev. Lett. **105**, 026601 (2010).
[27]N. L. Schneider, J. T. Lü, M. Brandbyge, and R. Berndt, Phys. Rev. Lett. **109**, 186601 (2012).
[28]R. Marty, C. Girard, A. Arbouet, and G. Colas des Francs, Chem. Phys. Lett. **532**, 100 (2012).
[29]U. Gavish, Y. Levinson, and Y. Imry, Phys. Rev. B **62**, R10637 (2000).
[30]R. Aguado and L. P. Kouwenhoven, Phys. Rev. Lett. **84**, 1986 (2000).
[31]A. V. Lebedev, G. B. Lesovik, and G. Blatter, Phys. Rev. B **81**, 155421 (2010).
[32]M. Brandbyge, J.-L. Mozos, P. Ordejon, J. Taylor, and K. Stokbro, Phys. Rev. B **65**, 165401 (2002).
[33]M. Paulsson and M. Brandbyge, Phys. Rev. B **76**, 115117 (2007).
[34]Y. Blanter and M. Buttiker, Phys. Rep. **336**, 1 (2000).
[35]J. M. Soler, E. Artacho, J. D. Gale, A. Garcia, J. Junquera, P. Ordejon, and D. Sanchez-Portal, J. Phys.: Condens. Matter **14**, 2745 (2002).
[36]J. P. Perdew, K. Burke, and M. Ernzerhof, Phys. Rev. Lett. **77**, 3865 (1996).
[37]S. Garcia-Gil, A. Garcia, N. Lorente, and P. Ordejon, Phys. Rev. B **79**, 075441 (2009).
[38]J. A. Scholl, A. Garca-Etxarri, A. L. Koh, and J. A. Dionne, Nano Lett. **13**, 564 (2013).
[39]K. J. Savage, M. M. Hawkeye, R. Esteban, A. G. Borisov, J. Aizpurua, and J. J. Baumberg, Nature (London) **491**, 574 (2012).
[40]W. W. Pai, H. T. Jeng, C. M. Cheng, C. H. Lin, X. D. Xiao, A. D. Zhao, X. Q. Zhang, G. Xu, X. Q. Shi, M. A. Van Hove *et al.*, Phys. Rev. Lett. **104**, 036103 (2010).
[41]P. Song, P. Nordlander, and S. Gao, J. Chem. Phys. **134**, 074701 (2011).
[42]M. Büttiker, Phys. Rev. B **45**, 3807 (1992).